MODELLING CROSS-LINKING IN COLLAGEN FIBRILS

by

Matthew Leighton

Submitted in partial fulfillment of the requirements
for the degree of Bachelor's of Science Honours

at

Dalhousie University
Halifax, Nova Scotia
December 20, 2019

© Copyright by Matthew Leighton,

Table of Contents

List of Figures

Abstract

Collagen fibrils are microscopic molecular ropes that are structural components in many animal tissues. We develop and explore an equilibrium coarse-grained model for the structural and mechanical properties of these cross-linked fibrils. We model enzymatic cross-links as anisotropic Gaussian chains, which allows us to approximate their free-energy contributions. We add additional terms in the free energy for the Frank elastic energy due to the orientation of collagen molecules within the fibril, for the surface tension, and phase-field crystal terms which account for the D-band density modulations observed along the length of collagen fibrils. We computationally minimize the sum of these free-energy terms with respect to imposed strain fields acting on the fibril to obtain equilibrium structures. Using this framework we investigate the effect of strain on various important structural and mechanical properties of a cross-linked fibril, such as the molecular director field, the stress-strain curve, and the D-band.

Acknowledgements

I would like to thank my supervisor professor Andrew Rutenberg for introducing me to the theory of cross-linked elastomers, and for guiding me along the way in this project. I would also like to thank professor Laurent Kreplak as well as Sam Cameron, and the rest of the Rutenberg group for many useful discussions and helpful feedback.

Chapter 1

Introduction

Collagen fibrils are molecular ropes, $\sim$ 1 to 100μm long [8], which are a principal structural component of many animal tissues such as tendons, bones, cartilage, and corneas [4][3][5]. They are composed of filaments of tropocollagen (the most abundant protein in the human body [9]), molecules around 300nm long [8].

Tropocollagen filaments can be modelled as being arranged in the fibril according to a double twist director field $\boldsymbol{n} = -\sin\psi(r)\hat{\boldsymbol{\phi}} + \cos\psi(r)\hat{\boldsymbol{z}}$ [6]. We express this molecular director field in cylindrical coordinates ($\boldsymbol{n} = \boldsymbol{n}(r, \phi, z)$). The function $\psi(r)$ is an r-dependent twist angle of $\boldsymbol{n}$ with respect to the $\hat{\boldsymbol{z}}$-axis, often approximated with one of two different functional forms: a constant angle approximation [17], and a constant angle gradient approximation [16].

Collagen fibrils can often be recognized by their characteristic D-band striations — periodic density modulations along the length of the fibril due to gaps in the spatial arrangement of the tropocollagen filaments. The collagen D-band phenomenon is well characterized experimentally (see e.g. [24], [7]), and has recently been modelled using a phase field liquid-crystal framework [10].

Inside the fibril, tropocollagen filaments are held together primarily by enzymatic cross-links, spring-like structures which connect two tropocollagen filaments at specific sites along their lengths. These cross-links are believed to provide much of the tensile strength of collagen fibrils [12]. Cross-links are formed in two different ways: Enzymatic cross-links (whose formation is catalyzed by the enzyme Lysyl oxidase), which are created during fibril formation, and cross-links formed due to advanced glycation end products (AGEs), which are created spontaneously due to ambient sugars long after fibril formation over a very slow time scale [18].

AGE-related cross-links have been associated with numerous human health problems. In particular, increased fibril cross-linking has been found to have a significant impact on biomechanical properties of the cornea such as elasticity and transparency

[11]. However, the impact of increased cross-linking in fibrils is not currently well-understood quantitatively.

Of particular interest is determining how collagen fibrils react to mechanical deformation. Stress strain curves for longitudinal stretching of collagen fibrils have been well-determined experimentally [24][31], but have yet to be accurately recovered by a theoretical model. We hope that incorporating the effects of intermolecular cross-linking, which have been ignored in previous modelling work [9][6][10], will improve our understanding of the mechanics of collagen fibrils.

There exists a rich mathematical framework built to model cross-linking in nematic liquid crystal elastomers [29]. Previous research into structural changes of nematic elastomers under strain has primarily focussed on helical director fields [28][26]. In this work we extend the framework to the double-twist director field of collagen fibrils, and the added context of a D-band density modulation. We will aim to understand the effect of strain on cross-linked fibrils, looking in particular at the molecular twist angle, the D-band amplitude, and the stress-strain curve.

Chapter 2

Modelling Framework

In order to model the structural properties of collagen fibrils we consider infinitely long fibrils, and focus primarily on the radial structure. We then consider the different contributions to a fibril's free energy per unit volume. This free energy is composed of a number of terms, detailed below. To obtain equilibrium fibril structural properties, we minimize this free energy subject to a given strain field.

2.0.1 A note on free energies per unit volume

Consider a free energy density $f(r)$ throughout a cylindrical fibril of radius R and length L. The total free energy within the fibril is

$$\widehat{E} = \int_0^{2\pi} \int_0^L \int_0^R r f dr dz d\phi = 2\pi L \int_0^R r f dr. \tag{2.1}$$

The free energy per unit volume, E, is the total free energy divided by the volume of the fibril ($V_f = \pi R^2 L$):

$$E = \widehat{E}/V_f = \frac{2\pi L}{\pi R^2 L} \int_0^R r f dr = \frac{2}{R^2} \int_0^R r f dr. \tag{2.2}$$

2.1 Frank Free Energy

The Frank free energy models the free energy contributions due to orientational molecular configurations of a liquid crystal. As used in previous collagen modelling work, the elastic Frank free energy density for a chiral liquid crystal system with a double twist director field $\boldsymbol{n} = -\sin(\psi(r))\hat{\boldsymbol{\phi}} + \cos(\psi(r))\hat{\boldsymbol{z}}$ is [9]

$$\begin{aligned} f_{\text{Frank}} = & \frac{1}{2} K_{22} \left(q - \psi' - \frac{\sin(2\psi)}{2r} \right)^2 \\ & + \frac{1}{2} K_{33} \frac{\sin^4(\psi)}{r^2} \\ & - \frac{1}{2} (K_{22} + k_{24}) \frac{1}{r} \frac{d}{dr} \left(\sin^2(\psi) \right). \end{aligned} \tag{2.3}$$

Here K_{22}, k_{24}, K_{33} are the Frank elastic constants, while the sign of q determines the preferred chirality of the fibril.

We will primarily make use of the Frank free energy per unit volume:

$$\begin{aligned} E_{\text{Frank}} &= \frac{2}{R^2}\int_0^R r f_{\text{Frank}} dr \\ &= \frac{2}{R^2}\int_0^R r\left(\frac{1}{2}K_{22}\left(q-\psi'-\frac{\sin(2\psi)}{2r}\right)^2+\frac{1}{2}K_{33}\frac{\sin^4(\psi)}{r^2}\right)dr \\ &- (K_{22}+k_{24})\frac{\sin^2\psi}{R^2}. \end{aligned} \tag{2.4}$$

2.2 Surface Energy

The surface energy per unit volume is

$$E_{\text{Surface}} = \frac{2\gamma}{R}, \tag{2.5}$$

where γ is a constant quantifying the surface tension of the fibril.

2.3 Phase Field Crystal Model for D-band Density Modulation

An important physical characteristic of collagen fibrils is the D-band, which is essentially a periodic density modulation along the length of the fibril. This phenomenon can be modelled using coarse-grained phase field crystal (PFC) theory [15], which accounts for free energy contributions due to periodic density modulations in crystalline materials. This framework has been previously adapted to the collagen double-twist ansatz [10], resulting in the following free energy per unit volume:

$$E_{\text{PFC}} = \frac{\Lambda\delta^2}{2R^2}\int_0^R\left(\frac{4\pi^2}{d_\parallel^2}-\eta^2\cos^2\psi(r)\right)^2 r\mathrm{d}r + \frac{\omega\delta^2}{2}\left(\frac{3\delta^2}{4}-\delta_0^2\right). \tag{2.6}$$

Here $d_\parallel$ is the expected D-band period in the absence of molecular twist, Λ characterizes the D-band stiffness, ω characterizes the energetics of D-band formation, and δ and η are the D-band amplitude and wavenumber, respectively. The first term in the above equation incentivizes the D-band period to match up with $d_\parallel$, while the second term allows a non-zero equilibrium value for the D-band amplitude.

2.4 Cross-Linking Theory

Here we derive a new free energy term describing anisotropic Gaussian cross-links under strain. The primary source for this is [29]. Published derivations for elastomeric free energy contributions due to cross-linking tend to jump straight from Equation 2.7 to the final line of 2.10, and from Equation 2.12 to 2.14. In the following two subsections I aim to fill in the blanks in the derivation and illuminate for the reader the origins of the key result (Equation 2.14).

2.4.1 Isotropic cross-linking

We model each cross-link as a polymer chain of length L and end-to-end distance $\boldsymbol{R}$. As such, the distribution of $\boldsymbol{R}$ is a Gaussian of the form

$$P(\boldsymbol{R}) = \left[\frac{3}{2\pi R_0^2}\right]^{3/2} \exp\left(\frac{-3}{2R_0^2}\boldsymbol{R}\cdot\boldsymbol{R}\right). \tag{2.7}$$

Here $R_0^2 = \ell_0 L$, where ℓ_0 is the effective step length of the polymer chain.

The free energy for a single cross-link with end-to-end distance $\boldsymbol{R}$ is entirely entropic, and is thus given by

$$\begin{aligned}\mathscr{F}(\boldsymbol{R}) &= -k_B T \ln P(\boldsymbol{R}) \\ &= \frac{3k_B T}{2R_0^2}\boldsymbol{R}\cdot\boldsymbol{R} - \frac{3k_B T}{2}\ln\left(\frac{3}{2\pi R_0^2}\right).\end{aligned} \tag{2.8}$$

We average this free energy over the probability distribution $P(\boldsymbol{R})$ of all cross-link orientations, which gives us

$$\begin{aligned}\langle\mathscr{F}\rangle &= \frac{3k_B T}{2R_0^2}\langle\boldsymbol{R}\cdot\boldsymbol{R}\rangle - \frac{3k_B T}{2}\ln\left(\frac{3}{2\pi R_0^2}\right) \\ &= \frac{3k_B T}{2R_0^2}\left(R_0^2\right) - \frac{3k_B T}{2}\ln\left(\frac{3}{2\pi R_0^2}\right) \\ &= \frac{3}{2}k_B T\left[1 + \ln\left(\frac{2\pi R_0^2}{3}\right)\right]\end{aligned} \tag{2.9}$$

for the free energy of the ensemble of configurations of a single cross-link. We find that we our cross-link free energy is almost equipartition, with a correction factor dependent on the mean cross-link end-to-end distance.

We now consider the effect of a strain on the cross-linked collagen fibril, which we quantify using the strain tensor, $\underline{\underline{\boldsymbol{\lambda}}}$. With regard to the cross-linking, the key effect

of the strain is to alter the end-to-end cross-link distance. The strain field causes the transformation $\boldsymbol{R}_{\text{new}} = \underline{\underline{\boldsymbol{\lambda}}}\boldsymbol{R}$. The new free energy per cross-link $\mathscr{F}(\boldsymbol{R}_{\text{new}})$ is of similar form to Eq. 2.7.

To calculate the new free energy per cross-link, we plug $\boldsymbol{R}_{\text{new}}$ into Eq. 2.8 and average over the pre-strain cross-linking distribution. The resulting free energy is

$$\begin{aligned}
\langle \mathscr{F} \rangle &= \frac{3k_BT}{2R_0^2} \langle \boldsymbol{R}_{\text{new}}^\top \cdot \boldsymbol{R}_{\text{new}} \rangle_{P(\boldsymbol{R})} \\
&= \frac{3k_BT}{2R_0^2} \langle \boldsymbol{R}^\top \cdot \underline{\underline{\boldsymbol{\lambda}}}^\top \cdot \underline{\underline{\boldsymbol{\lambda}}} \cdot \boldsymbol{R} \rangle_{P(\boldsymbol{R})} \\
&= \frac{3k_BT}{2R_0^2} \left\langle \text{Tr}\left[\boldsymbol{R}^\top \cdot \underline{\underline{\boldsymbol{\lambda}}}^\top \cdot \underline{\underline{\boldsymbol{\lambda}}} \cdot \boldsymbol{R} \right] \right\rangle_{P(\boldsymbol{R})} \\
&= \frac{3k_BT}{2R_0^2} \left\langle \text{Tr}\left[\underline{\underline{\boldsymbol{\lambda}}}^\top \cdot \underline{\underline{\boldsymbol{\lambda}}} \cdot \boldsymbol{R} \cdot \boldsymbol{R}^\top \right] \right\rangle_{P(\boldsymbol{R})} \\
&= \frac{3k_BT}{2R_0^2} \text{Tr}\left[\underline{\underline{\boldsymbol{\lambda}}}^\top \cdot \underline{\underline{\boldsymbol{\lambda}}} \cdot \left\langle \boldsymbol{R} \cdot \boldsymbol{R}^\top \right\rangle_{P(\boldsymbol{R})} \right] \\
&= \frac{3k_BT}{2R_0^2} \text{Tr}\left[\underline{\underline{\boldsymbol{\lambda}}}^\top \cdot \underline{\underline{\boldsymbol{\lambda}}} \cdot \left(\frac{R_0^2}{3} \underline{\underline{\delta}} \right) \right] \\
&= \frac{1}{2} k_BT \text{Tr}\left[\underline{\underline{\boldsymbol{\lambda}}}^\top \cdot \underline{\underline{\boldsymbol{\lambda}}} \right].
\end{aligned} \tag{2.10}$$

Here we have omitted an additive constant, which we shall continue to do going forward.

2.4.2 Anisotropic cross-linking

To model anisotropic cross-linking, we replace the scalar effective step length ℓ_0 with the tensor

$$\underline{\underline{\boldsymbol{\ell}}}_0 = \ell_\perp \underline{\underline{\boldsymbol{\delta}}} + [\ell_\parallel - \ell_\perp] \boldsymbol{n_0} \otimes \boldsymbol{n_0}, \tag{2.11}$$

which describes the anisotropy of the cross-link network. Here $\ell_\parallel$ is the effective step length parallel to the local director field $\boldsymbol{n_0}$, while $\ell_\perp$ is the perpendicular effective step length. We also define the dimensionless ratio $\zeta = \ell_\parallel / \ell_\perp$, which we will later make use of in order to simplify expressions. We then have the end-to-end cross-link distance distribution

$$P(\boldsymbol{R}) = \left[\left(\frac{3}{2\pi L} \right)^3 \frac{1}{\text{Det}[\underline{\underline{\boldsymbol{\ell}}}_0]} \right]^{1/2} \exp\left(-\frac{3}{2L} \boldsymbol{R}^\top \underline{\underline{\boldsymbol{\ell}}}_{\boldsymbol{0}}^{-\boldsymbol{1}} \boldsymbol{R} \right). \tag{2.12}$$

Note here that $\underline{\underline{\boldsymbol{\ell}}}_0^{-1} = 1/\ell_\perp \underline{\underline{\boldsymbol{\delta}}} + [1/\ell_\parallel - 1/\ell_\perp]\boldsymbol{n_0} \otimes \boldsymbol{n_0}$. We show that this is the correct form for the inverse of $\underline{\underline{\boldsymbol{\ell}}}_0$ in the Appendix.

Now, we again consider the effect of a strain field $\underline{\underline{\boldsymbol{\lambda}}}$ acting on the fibril. The free energy per cross-link $\mathscr{F}(\boldsymbol{R}_{\text{new}})$ (where $\boldsymbol{R}_{\text{new}} = \underline{\underline{\boldsymbol{\lambda}}}\boldsymbol{R}$) is analogous to Eq. 2.10. Thus, as before, we average $\mathscr{F}(\boldsymbol{R}_{\text{new}})$ with respect to the probability distribution $P(\boldsymbol{R})$ from Eq. 2.12. This gives us

$$\begin{aligned}
\langle \mathscr{F} \rangle &= \frac{3k_BT}{2L} \langle \boldsymbol{R}_{\text{new}}^\top \cdot \underline{\underline{\boldsymbol{\ell}}}^{-1} \cdot \boldsymbol{R}_{\text{new}} \rangle_{P(\boldsymbol{R})} \\
&= \frac{3k_BT}{2L} \langle \boldsymbol{R}^\top \cdot \underline{\underline{\boldsymbol{\lambda}}}^\top \cdot \underline{\underline{\boldsymbol{\ell}}}^{-1} \cdot \underline{\underline{\boldsymbol{\lambda}}} \cdot \boldsymbol{R} \rangle_{P(\boldsymbol{R})} \\
&= \frac{3k_BT}{2L} \text{Tr}\left[\underline{\underline{\boldsymbol{\lambda}}}^\top \cdot \underline{\underline{\boldsymbol{\ell}}}^{-1} \cdot \underline{\underline{\boldsymbol{\lambda}}} \cdot \langle \boldsymbol{R}^\top \cdot \boldsymbol{R} \rangle_{P(\boldsymbol{R})} \right] \\
&= \frac{3k_BT}{2L} \text{Tr}\left[\underline{\underline{\boldsymbol{\lambda}}}^\top \cdot \underline{\underline{\boldsymbol{\ell}}}^{-1} \cdot \underline{\underline{\boldsymbol{\lambda}}} \cdot \left(\frac{L}{3} \underline{\underline{\boldsymbol{\ell}}}_0 \right) \right] \\
&= \frac{1}{2} k_BT \ \text{Tr}[\underline{\underline{\boldsymbol{\ell}}}_0 \cdot \underline{\underline{\boldsymbol{\lambda}}}^\top \cdot \underline{\underline{\boldsymbol{\ell}}}^{-1} \cdot \underline{\underline{\boldsymbol{\lambda}}}].
\end{aligned} \tag{2.13}$$

From here, we can get a free energy density due to the cross-linking by multiplying the average free energy per cross-link ($\langle \mathscr{F} \rangle$) by the cross-link density within the fibril, ρ. We then have the standard anisotropic elastomeric contribution[29]:

$$\boxed{f_{\text{Cross-Link}} = \frac{1}{2} \rho k_BT \ \text{Tr}(\underline{\underline{\boldsymbol{\ell}}}_0 \underline{\underline{\boldsymbol{\lambda}}}^\top \underline{\underline{\boldsymbol{\ell}}}^{-1} \underline{\underline{\boldsymbol{\lambda}}}).} \tag{2.14}$$

We define $\mu = \rho k_BT$, which is the elastic shear modulus for the fibril [27]. This parameter has been found to have a wide range of values experimentally, but observations generally fall in the range of $10^6 - 10^8$ Pa for *in vivo* collagen fibrils [13][25].

The free energy per unit volume is then

$$E_{\text{Cross-Link}} = \frac{2}{R^2} \int_0^R r f_{\text{Cross-Link}} dr = \frac{\mu}{R^2} \int_0^R r \ \text{Tr}(\underline{\underline{\boldsymbol{\ell}}}_0 \underline{\underline{\boldsymbol{\lambda}}}^\top \underline{\underline{\boldsymbol{\ell}}}^{-1} \underline{\underline{\boldsymbol{\lambda}}}) dr, \tag{2.15}$$

where $R = R_0/\sqrt{\epsilon}$ is the post-strain fibril radius, and R_0 is the pre-strain equilibrium radius.

2.4.3 Non-Gaussian approaches

A limitation of our Gaussian cross-link approach is that arbitrarily large deformations of the cross-links are permitted with non-zero probability. In reality, the cross-links

will have some maximum length beyond which further stretching is impossible while remaining intact.

First order corrections to the cross-linking free energy due to finite extensibility effects have been derived for both isotropic [21] and anisotropic cross-links [22]. These models assume the cross-links to be polymer chains consisting of a fixed number of monomer links with known dimensions. In the anisotropic case, the average free energy per cross-link chain with N units of length b (in the direction of $\boldsymbol{n}$) is

$$\langle \mathscr{F} \rangle = k_B T \left[\frac{1}{2} \underline{\underline{\boldsymbol{\ell}}} : \underline{\underline{\boldsymbol{L}}} - \frac{54}{Nb^2} \underline{\underline{\boldsymbol{\ell}}}^{-1} : \underline{\underline{\underline{\underline{\boldsymbol{B}}}}} : \underline{\underline{\boldsymbol{L}}} + \frac{27}{Nb^2} \underline{\underline{\boldsymbol{L}}} : \underline{\underline{\underline{\underline{\boldsymbol{B}}}}} : \underline{\underline{\boldsymbol{L}}} + \boldsymbol{O}(N^{-2}) + \text{const.} \right], \tag{2.16}$$

where $\underline{\underline{\boldsymbol{L}}} = \underline{\underline{\boldsymbol{\ell}}}^{-1} \cdot \underline{\underline{\boldsymbol{\lambda}}} \cdot \underline{\underline{\boldsymbol{\ell}}}_0 \cdot \underline{\underline{\boldsymbol{\lambda}}}^{\top} \cdot \underline{\underline{\boldsymbol{\ell}}}^{-1}$, and $\underline{\underline{\underline{\underline{\boldsymbol{B}}}}}$ is a $4th$-rank tensor dependent on N, b, ζ, and $\boldsymbol{n}$. Here ":" denotes the double inner product.

The main advantage of the Gaussian cross-link model, in addition to ease of computation and the existence of exact results, is that we can describe anisotropic cross-links with only one parameter, ζ. To account for finite extensibility effects, we would need to somehow determine approximate values of the additional constants N and b. The reduced parameter freedom obtained using the Gaussian approximation allows us to obtain results dependent on fewer assumptions. Further, we expect finite extensibility effects to be negligible for small strains, which are the main focus of this work. Thus, we ignore finite extensibility effects for now, but note that we expect them to become relevant at high strain.

2.5 Details

2.5.1 Anisotropy tensor

In cylindrical coordinates $(\hat{r}, \hat{\phi}, \hat{z})$, and given the double-twist director field $\boldsymbol{n_0}$, the cross-link anisotropy tensor $\underline{\underline{\boldsymbol{\ell}}}_0$ is

$$\begin{aligned} \underline{\underline{\boldsymbol{\ell}}}_0 &= \ell_\perp \underline{\underline{\boldsymbol{\delta}}} + [\ell_\parallel - \ell_\perp] \boldsymbol{n_0} \otimes \boldsymbol{n_0} \\ &= \ell_\perp \begin{bmatrix} 1 & 0 & 0 \\ 0 & 1 + (\zeta - 1)\sin^2\psi & (1-\zeta)\sin\psi\cos\psi \\ 0 & (1-\zeta)\sin\psi\cos\psi & 1 + (\zeta-1)\cos^2\psi \end{bmatrix}. \end{aligned} \tag{2.17}$$

We take the post-strain director field to be

$$\boldsymbol{n} = -\sin(\psi^*(r))\hat{\boldsymbol{\phi}} + \cos(\psi^*(r))\hat{\boldsymbol{z}}, \tag{2.18}$$

where $\psi^*(r)$ is the new double-twist angle that will be determined by minimizing the free energy. Thus the post-strain anisotropy tensor is

$$\begin{aligned}\underline{\underline{\boldsymbol{\ell}}}^{-1} &= 1/\ell_\perp \underline{\underline{\boldsymbol{\delta}}} + [1/\ell_\parallel - 1/\ell_\perp]\boldsymbol{n}\otimes\boldsymbol{n} \\ &= \ell_\perp^{-1}\begin{bmatrix} 1 & 0 & 0 \\ 0 & 1+(\zeta^{-1}-1)\sin^2\psi^* & (1-\zeta^{-1})\sin\psi^*\cos\psi^* \\ 0 & (1-\zeta^{-1})\sin\psi^*\cos\psi^* & 1+(\zeta^{-1}-1)\cos^2\psi^* \end{bmatrix}.\end{aligned} \tag{2.19}$$

2.5.2 Strain field

We consider two forms for the strain tensor.

Pure Deformation

We consider a purely longitudinal strain with a deformation $u_z = \epsilon z$, ignoring contributions from shear strain. As is standard practice when modelling the straining of nematic elastomers, we consider only deformations that maintain a constant volume [29], which is equivalent to the condition $\mathrm{Det}(\underline{\underline{\boldsymbol{\lambda}}}) = 1$ [20]. Thus we have the fully imposed strain tensor

$$\underline{\underline{\boldsymbol{\lambda}}} = \begin{bmatrix} \frac{1}{\sqrt{\epsilon}} & 0 & 0 \\ 0 & \frac{1}{\sqrt{\epsilon}} & 0 \\ 0 & 0 & \epsilon \end{bmatrix}. \tag{2.20}$$

Shear Deformation

We also consider another form for the strain tensor:

$$\underline{\underline{\boldsymbol{\lambda}}} = \begin{bmatrix} \frac{1}{\sqrt{\epsilon}} & 0 & 0 \\ 0 & \frac{1}{\sqrt{\epsilon}} & \kappa \\ 0 & 0 & \epsilon \end{bmatrix}, \tag{2.21}$$

which adds a rotation around the $\boldsymbol{z}$-axis in order to model the effects of rotational shear forces caused by pulling on a fibril [30]. Imposing a value of κ is not necessary, it can be determined analytically by minimizing $f_{\text{Cross-Link}}$ with respect to κ [28][26]. Note that in general, $\kappa \equiv \kappa(\epsilon, r, \psi(r), \zeta)$.

Incompressibility

Note that we maintain a constant fibril volume during the strain by letting $R \to R/\sqrt{\epsilon}$. We also let $\eta \to \eta/\epsilon$, *i.e.* we directly strain the D-band by the same amount as the fibril. As a result, the phase field crystal free energy, E_{PFC}, will also depend on $\underline{\underline{\boldsymbol{\lambda}}}$.

2.5.3 Total free energy

The total free energy per unit volume for a cross-linked collagen fibril is then

$$E_{\text{Total}} = E_{\text{Frank}} + E_{\text{Surface}} + E_{\text{PFC}} + E_{\text{Cross-Link}}, \tag{2.22}$$

with functional dependencies (ignoring constants like K_{ij}, γ, Λ, and ω) as follows:

$$E_{\text{Frank}} \equiv E_{\text{Frank}}(R, \psi^*(r)), \tag{2.23a}$$

$$E_{\text{Surface}} \equiv E_{\text{Surface}}(R), \tag{2.23b}$$

$$E_{\text{PFC}} \equiv E_{\text{PFC}}(R, \psi^*(r), \delta, \underline{\underline{\boldsymbol{\lambda}}}), \tag{2.23c}$$

$$E_{\text{Cross-Link}} \equiv E_{\text{Cross-Link}}(R, \psi(r), \psi^*(r), \underline{\underline{\boldsymbol{\lambda}}}, \zeta, \mu). \tag{2.23d}$$

In order to determine the post-strain equilibrium twist angle, we minimize the total free energy with respect to $\psi^*(r)$ for a given strain field (see Section 2.7 for details).

The longitudinal stress (σ_{zz}) in the fibril due to a longitudinal strain (ϵ) is then given by [20]

$$\sigma_{zz} = \frac{\partial E_{\text{Total}}}{\partial \epsilon}. \tag{2.24}$$

2.5.4 Equilibrium twist phases

We consider two different functional forms for the initial double-twist angle of the director field that approximate the equilibrium collagen fibril phases found by Cameron *et al.* [10]

The first of these is a linear twist phase, where $\psi(r) = \alpha r$. For this phase we use a fibril radius of $R_0^L = 25\text{nm}$.

The second equilibrium fibril configuration is a constant twist phase, where

$$\psi(r) = \beta \mathbb{1}_{[\widehat{R}_0^C, R_0^C]} = \begin{cases} 0, & \text{if } r < \widehat{R}_0^C \\ \beta, & \text{if } \widehat{R}_0^C \leq r \leq R_0^C. \end{cases} \tag{2.25}$$

We take $R_0^C = 100\text{nm}$, and $\widehat{R}_0^C = \frac{1}{10} R_0^C$. the region in the center of the fibril where $r < R_0^C$ represents a molten core [10].

We choose our model parameters to match the conditions that allow these two phases to coexist [10].

2.6 Dimensional Analysis and Parameter Values

Using dimensional analysis we can reduce the number of parameters and variables required by our model. We then have 8 dimensionless parameters:

$$\tilde{K}_{33} = \frac{K_{33}}{K_{22}}, \tag{2.26a}$$

$$\tilde{k}_{24} = \frac{k_{24}}{K_{22}}, \tag{2.26b}$$

$$\tilde{\gamma} = \frac{\gamma}{K_{22} q}, \tag{2.26c}$$

$$\tilde{\Lambda} = \frac{2\Lambda \delta_0^2}{3 K_{22} q^2 d_\parallel^4}, \tag{2.26d}$$

$$\tilde{\eta} = \eta d_\parallel, \tag{2.26e}$$

$$\tilde{\omega} = \frac{2\omega \delta_0^4}{3 K_{22} q^2}, \tag{2.26f}$$

$$\tilde{\mu} = \frac{\mu}{K_{22} q^2}, \tag{2.26g}$$

$$\zeta \text{ (already dimensionless).} \tag{2.26h}$$

We also have the following dimensionless variables used to characterize our fibrils:

$$\tilde{E} = \frac{E}{K_{22} q^2}, \tag{2.27a}$$

$$\tilde{R} = Rq, \tag{2.27b}$$

$$\tilde{r} = rq, \tag{2.27c}$$

$$\tilde{\psi}(\tilde{r}) = \psi(r), \tag{2.27d}$$

$$\tilde{\delta} = \sqrt{3/2}\frac{\delta}{\delta_0}, \tag{2.27e}$$

$$\epsilon \text{ (already dimensionless)}. \tag{2.27f}$$

Unless otherwise specified, we take $\tilde{K}_{33} = 30$, $\tilde{k}_{24} = 0.5$, $\tilde{\gamma} = 0.04$, $\tilde{\Lambda} = 600$, $\tilde{\omega} = 20$. For the constant twist phase, we take $\tilde{\eta}_C = 2\pi/0.985$, while for the linear twist phase, we take $\tilde{\eta}_L = 2\pi/0.996$ [10]. We will explore the roles of the initial twist angle $\psi(r)$ (via our imposed functional form parameters, α and β), the strain ϵ, and the two parameters describing the cross-linking: ζ and μ.

We then have the following dimensionless equation for the total free energy per unit volume:

$$\begin{aligned}\tilde{E}_{\text{Total}} = \frac{2}{\tilde{R}^2}\int_0^{\tilde{R}} \tilde{r}\left(\frac{1}{2}\left(1-\tilde{\psi}'-\frac{\sin(2\tilde{\psi})}{2\tilde{r}}\right)^2 + \frac{\tilde{K}_{33}\sin^4\tilde{\psi}}{2\tilde{r}^2}\right)dr \\ + \frac{\tilde{\Lambda}\tilde{\delta}^2}{2\tilde{R}^2}\int_0^{\tilde{R}} \tilde{r}\left(r\pi^2 - \tilde{\eta}^2\cos^2\tilde{\psi}\right)^2 dr + \frac{\tilde{\omega}\tilde{\delta}^2}{2}\left(\frac{\tilde{\delta}^2}{2}-1\right) \\ - (1+\tilde{k}_{24})\frac{\sin^2\tilde{\psi}(\tilde{R})}{\tilde{R}^2} + \frac{2\tilde{\gamma}}{\tilde{R}} + \frac{\tilde{\mu}}{\tilde{R}^2}\int_0^{\tilde{R}} \tilde{r}\ \text{Tr}(\underline{\underline{\boldsymbol{\ell}}}_0\underline{\underline{\boldsymbol{\lambda}}}^\top\underline{\underline{\boldsymbol{\ell}}}^{-1}\underline{\underline{\boldsymbol{\lambda}}})dr.\end{aligned} \tag{2.28}$$

2.7 Numerical Minimization Procedures

For a given longitudinal strain, we minimize the total free energy in equation 2.28 with respect to either α^* or β^*, the parameters of the post-strain twist angle functions for the linear and constant twist phases respectively. In section 3.2.2 we vary the D-band amplitude $\tilde{\delta}$ in addition to the twist-angle parameter. I wrote code to compute this total free energy and perform the minimization, for which I employed the particle swarm optimization (PSO) algorithm [14], as implemented in the *pyswarm* Python package (see https://pythonhosted.org/pyswarm). The PSO algorithm is effective for determining global minima in rough optimization landscapes, and can handle simultaneous minimization with respect to multiple parameters.

Chapter 3

Results

3.1 Elastic Properties in the Absence of a D-band

We initially consider the limit $\tilde{\delta} = 0$, which corresponds to a complete absence of D-band modulation within the fibril. We also consider the 'pure deformation' strain field as described in Eq 2.20. We begin by looking at the behaviour of the molecular director field under strain. Figure 3.1 shows how the average double-twist angle ($\langle\psi\rangle$) throughout the fibril varies with strain.

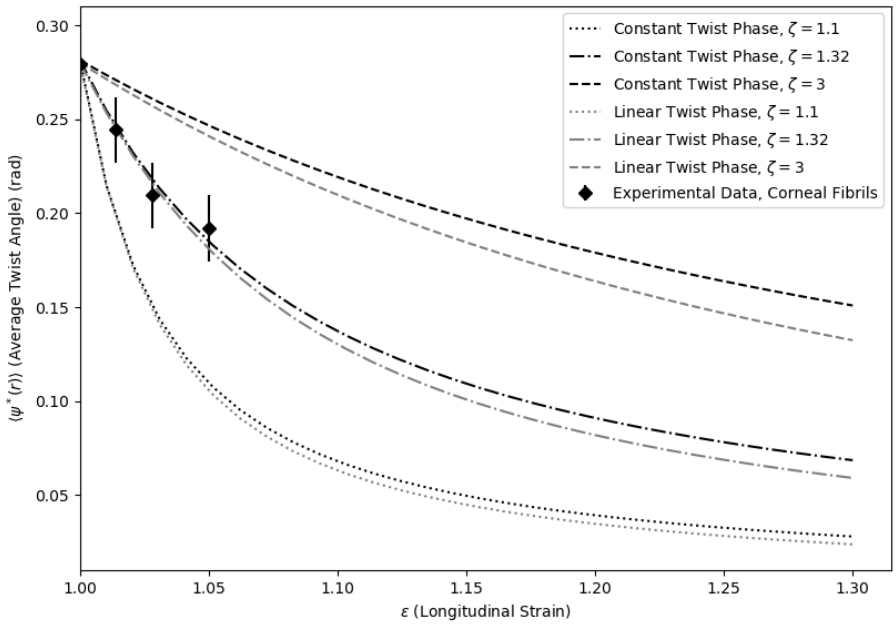

Figure 3.1: We plot the average twist angle as a function of strain for fibrils with a variety of different values of ζ, and $\tilde{\delta} = 0$. We take $\mu = 100$MPa. An initial average twist angle of 16° is imposed in order to compare with experimental data from [2].

It is clear that the behaviour of $\langle\psi\rangle$ is highly dependent on the cross-link anisotropy parameter, ζ. Note that in models of liquid-crystal elastomers, ζ is generally assumed to take a value between 1 and 10 [29][30]. In order to further constrain our estimate of

ζ, we compare our model outputs with experimental data from [2], a study in which the average twist angle of tropocollagen filaments within corneal fibrils was measured for several different strain values using the technique of small-angle X-ray scattering. To compare with the data, we impose the equilibrium pre-strain average twist seen in the experiment to both the linear and constant twist-phase fibrils in our model. From Figure 3.1 we see that for $\zeta \approx 1.3$ we fit the experimental data quite well (by eye). Note also that we see the constant twist phase better approximate the data than the linear twist phase. This is of particular interest since we expect the constant twist phase to better represent corneal fibrils [10]. We note that the strain-dependence of the twist angle is fairly independent of μ as long as $\mu >> K_{22}q^2 \approx 96$Pa.

We can now compute stress-strain curves for both of our fibril phases. Figure 3.2 compares the stress-strain curves computed from our model to both experimental data from [24] as well as to an analytic result for the stress-strain curve of an isotropic cross-linked rubber (see Appendix A.2),

$$\sigma(\epsilon) = \mu\left(\epsilon - \frac{1}{\epsilon^2}\right). \tag{3.1}$$

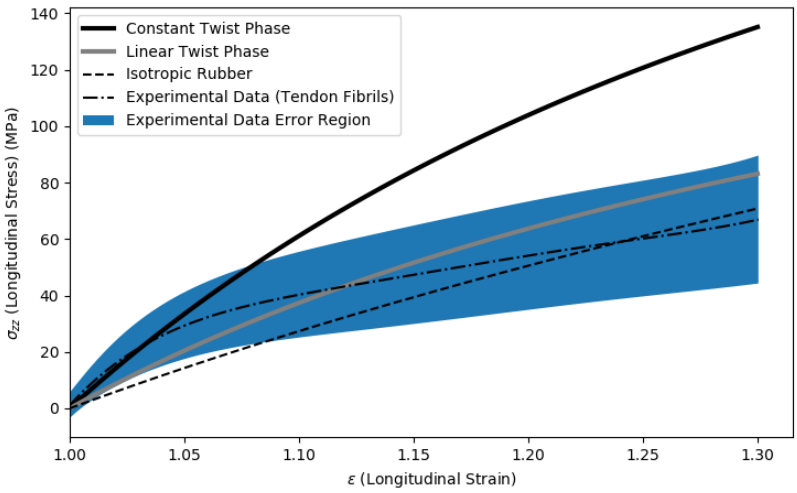

Figure 3.2: We plot stress-strain curves for the linear and constant twist fibril phases with $\mu = 100$MPa and $\zeta = 1.32$. We compare these curves to an analytic result for the stress-strain curve of an isotropic rubber with the same value of μ, as well as experimental data from [24] where we take the average of 11 stress-strain curves from bovine extensor tendon fibrils of comparable radius to our linear twist phase.

We find that our anisotropic double-twist fibril phases are both more rigid than an isotropic rubber with the same cross-linking density. Further, we find that the

constant twist phase is significantly more rigid than the linear twist phase. Recalling that we expect the constant twist phase to correspond approximately to corneal fibrils and the linear phase to approximate tendon fibrils, this result seems fairly intuitive given that on the macroscopic scale human corneas are generally more rigid than human tendons [1].

The experimental data shown in Figure 3.2 is the mean of 11 stress-strain curves measured from bovine extensor fibrils [24]. These 11 were selected for radii close to that of our linear twist phase from among approximately 40 available curves (see Section A.3). We note that there is some parameter freedom for the elastic shear modulus, μ, which controls the magnitude of the stress response to strain. For collagen fibrils we expect 3MPa$\leq \mu$MPa$\leq$ 300.

We find that the the stress strain curve of our linear twist phase with $\mu = 100$MPa fits the data fairly well for ϵ up to about 1.3. This is all we can reasonably expect from our equilibrium model, as beyond 15-20% strain the fibril deformation is no longer thought to be an approximately equilibrium process [19]. We see a noteworthy divergence from the experimental curve for $\epsilon < 1.05$. We expect this is due to our arbitrary constraint of $\tilde{\delta} = 0$, where experimentally $\tilde{\delta}$ has been found to fluctuate in that strain region [7].

3.1.1 Shear Deformation

We have also examined the elastic properties of fibrils in the $\tilde{\delta} = 0$ limit using the strain field from Equation 2.21, which adds a term to the strain tensor to account for shear deformation in the fibril. However, with the inclusion of this shear term, we find that under strain the twist angle inside the fibril oscillates about $\psi = 0$ (not shown) with a frequency that increases with the anisotropy parameter, ζ. This result is clearly not biologically relevant, as can be clearly seen by examining the experimental data from [2], which found a monotonically decreasing twist angle with strain. This could be an artefact of the simple twist angle functions we have used.

3.2 Incorporating the D-band

3.2.1 Imposing a constant D-band amplitude

We now consider fibrils with $\tilde{\delta} > 0$. However, we initially impose a D-band amplitude that is constant with strain. For the constant twist phase, we take $\tilde{\delta}_C = 0.998$, while for the linear twist phase, we take $\tilde{\delta}_L = 0.975$ [10]. A constant D-band with strain is consistent with many experimental results, such as [23], which found that the D-band was still present at 25% strain.

Rather than imposing an initial twist angle as in the previous section, we minimize the total free energy with respect to the twist angle in the absence of strain. We then use these equilibrium twist angles as our initial conditions prior to the application of strain. Note that we do not see an initial twist nearly as high as was observed in [2] (See Figure 3.1). This is likely a limitation due to our imposed twist angle functional forms.

We can then examine the the response of the fibril to strain. Figures 3.3 and 3.4 show our results for $\mu = 100$MPa and $\mu = 10$MPa respectively.

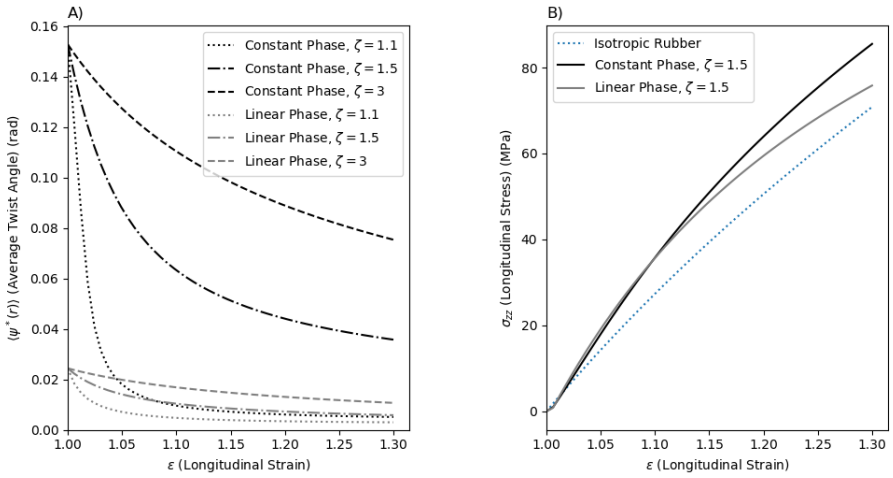

Figure 3.3: For $\mu = 100$MPa, we show **A)** The effect of strain on average twist angle throughout the fibril for both phases and various values of ζ and **B)** Stress-strain curves for both twist phases. Note that the stress-strain curves for both phases are essentially independent of ζ. We impose a constant D-band amplitude.

We find that the addition of the D-band causes several deviations in results from the $\tilde{\delta} = 0$ limit. In particular, we find that with the addition of the D-band causes

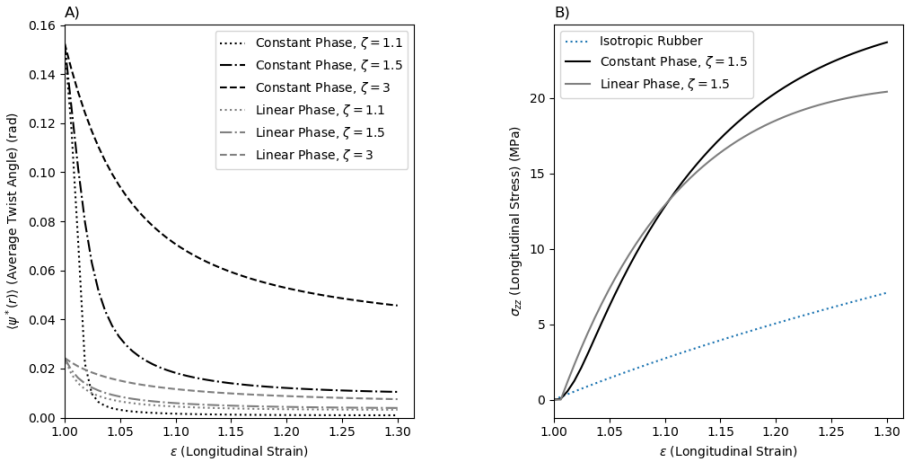

Figure 3.4: For $\mu = 10$MPa, we show **A)** The effect of strain on average twist angle throughout the fibril for both phases and various values of ζ and **B)** Stress-strain curves for both twist phases. We impose a constant D-band amplitude.

the stress-strain curves for the two twist phases to converge for strain up to about 20%. We then see the constant twist phase show increased rigidity compared to the linear twist phase for higher strain. We still find a significant discrepancy between the stress-strain response for our modelled fibrils and the analytic result for an isotropic rubber.

We find that as we decrease the ratio of $\tilde{\mu}$ to $\tilde{\Lambda}$, we see increased non-linear effects in the fibril stress-strain response. $\tilde{\mu}/\tilde{\Lambda} \approx 1700$ in Figure 3.3, but only ≈ 17 in Figure 3.4, where we see the stress-strain curve almost completely flatten out for high strain. For even lower $\tilde{\mu}/\tilde{\Lambda}$ we see the stress strain response of the fibril begin to decrease at high strain (not shown), which would lead to plastic behaviour [20]. We also note that decreasing $\tilde{\mu}/\tilde{\Lambda}$ causes the average twist angle throughout the fibril to decrease much faster with strain.

A D-band that stays constant with strain is not, however, biologically relevant, as there is evidence that the D-band disapears under strain. In the next section we examine the interaction of longitudinal strain with the D-band amplitude.

3.2.2 Effect of strain on the D-band

We now allow the D-band amplitude ($\tilde{\delta}$) to vary freely, giving our modelled fibrils an additional degree of freedom. Thus to determine equilibrium fibril conditions, we

minimize the total free energy of a fibril with respect to both $\psi(r)$ and $\tilde{\delta}$. Figure 3.5 shows equilibrium fibril conditions in the absence of strain for both phases across a wide range of fibril radii. Note that in order to find non-zero values at equilibrium for both the twist angle and the D-band amplitude, we are forced to depart from the PFC parameters used in [10]. We find that we can recover a non-zero molecular twist and D-band with $\Lambda = \omega = 100$. Once again though, we do not see an initial twist nearly as high as was observed in [2].

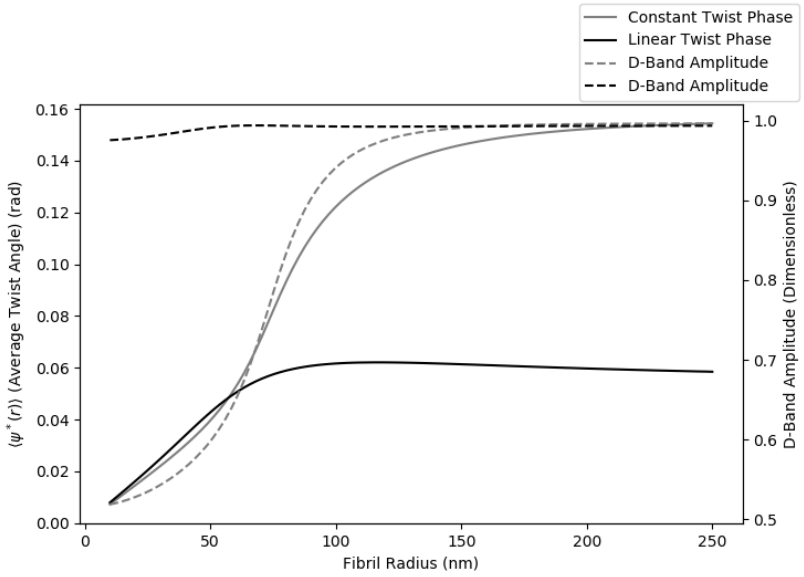

Figure 3.5: Equilibrium twist angles and free energies for the constant and linear twist phases in the absence of strain. We allow both the twist angle $\psi(r)$ and the D-band amplitude $\tilde{\delta}$ to vary. Note that here we take $\tilde{\Lambda} = \tilde{\omega} = 100$.

Starting from the these equilibrium fibril structures, we then once again compute the effects of a longitudinal strain on various fibril properties. Figure 3.6 shows stress-strain curves, along with the strain-response of the average twist angle and D-band amplitude.

We find that the applied strain eliminates the D-band very quickly, with it disappearing before 3% strain for all parameter values we examined. This prediction appears to be reflective of real fibril dynamics: previous experimental results have found that D-band striations in a fibril disappear by 4% applied strain [7]. The strain-response of the molecular twist angle is quite similar to our earlier results, modulo some bumps caused by the non-smooth vanishing of the D-band amplitude.

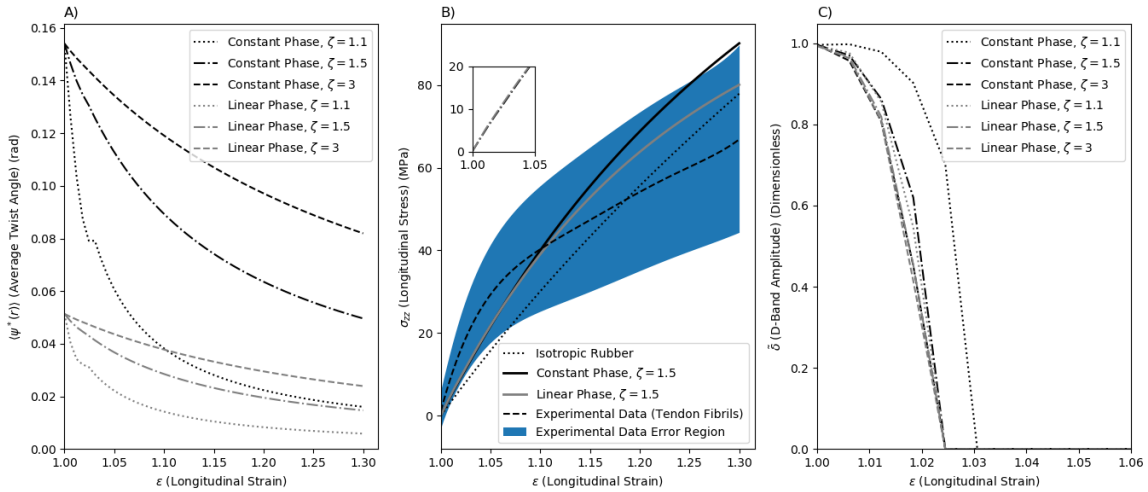

Figure 3.6: We show the effect of longitudinal strain on **A)** The average twist angle throughout the fibril, **B)** Stress throughout the fibril, and **C)** The D-band amplitude for both phases and various values of ζ. Note that here we take $\tilde{\Lambda} = \tilde{\omega} = 100$, and $\mu = 110$MPa. **B)** also includes experimental data from [24].

Looking next at the stress-strain curves, we see that the two fibril phases are less rigid than an isotropic rubber, for small strain, but become more rigid for higher strain. At high strain, we also see separation between the two phases. As in the $\tilde{\delta} = 0$ limit, we again are able to fit experimental stress-strain curves for strain up to about 30%. We find though that we need to use a higher value of μ (110MPa) to do this. This indicates that D-banded fibrils are less rigid than fibrils without a D-band.

Chapter 4

Discussion

We have added a free energy term describing the effects of intermolecular cross-links to an existing equilibrium coarse-grained model for collagen fibrils. Using this model, we have been able to determine the effects of strain on the structure of the fibril, as well as by extension the stress-strain curve.

In the $\tilde{\delta} = 0$ limit (no D-band), we are able to fit experimental data showing the change of the molecular twist angle with strain. This allows us to effectively constrain the cross-link anisotropy parameter ζ, as we find the shape of the $\langle\psi\rangle$-strain curve to be highly dependent on ζ. With a non-zero and varying D-band, however, we fail to see an equilibrium twist angle as high as that observed experimentally. We hope that by allowing a non-imposed twist angle function in future work we will be able to recover a greater initial twist, which will allow us to constrain the anisotropy parameter for D-banded fibrils.

When we allow the D-band amplitude to vary freely in addition to the molecular twist angle, we find that the D-band completely disappears (Figure 3.6C) after very low strain (around 3%), a finding consistent with quasi-static mechanical extension experiments. This is a new result arising from the interaction of intermolecular cross-linking with the D-band density modulation: previous work modelling non-cross-linked fibrils with a PFC-based D-band model did not see this effect.

We find that with or without the D-band, we can fit experimental stress-strain curves fairly well with similar cross-link densities, especially for $5-20\%$ strain. We see divergence from the experimental data at large strain, which is to be expected given the equilibrium nature of our model. Comparing the stress-strain curves from Figure 3.2 ($\tilde{\delta} = 0$ limit) with those from Figure 3.6 (freely varying $\tilde{\delta}$), we find that D-banded fibrils are less rigid than non-D-banded fibrils with the same cross-link density. This is likely due to the non-fixed D-band amplitude which, by decreasing, absorbs some of the strain applied to the fibril. We further note that imposing a constant D-band

with strain results in a flattening of the stress-curve with high strain, a feature which is found in experimental curves.

In conclusion, from our results here we see that intermolecular cross-linking has a very significant effect on fibril structure and elasticity under strain. In accounting for these cross-links, we have been able to gain a better understanding of how collagen fibrils respond to longitudinal strain.

4.1 Future Work

The logical next step (planned for next term) in this project is to consider a general twist angle function $\psi(r)$, rather than the imposed functional forms we have used here. To do this we will need to solve (numerically) the Euler-Lagrange equation at each value of ϵ in order to find the function $\psi(r)$ that minimizes the fibril free energy.

A better understanding of the interplay between the fibril D-band and the cross-linking is required. We would ideally like to understand if the behaviour of the D-band amplitude under strain is something that can be controlled by our various parameters.

In addition, we would like to understand the effects of shear forces in the fibril that occur during a longitudinal extension. I suspect that this will require the general twist angle function.

We would also like to look more at additional mechanical properties of cross-linked collagen fibrils. For instance, we could compute Young's modulus, as well as the mechanical anisotropy, which is the ratio of Young's modulus to the elastic shear modulus, μ [32]. Understanding how these properties are impacted by the cross-linking anisotropy parameter ζ is of significant interest.

Further, due to time constraints, we were not able to fully explore the parameter space spanned by μ, Λ, and ω. These are all parameters with a fairly wide range of possible values, so a better understanding of how they interact would be useful.

4.2 Open Questions

One limitation of the Gaussian chain model of cross-linking is that this model allows arbitrarily large end-to-end cross-link lengths to occur with non-zero probability. In reality, the cross-links are polymer chains consisting of some number N of monomer

links. Thus there is a maximum limit to the possible extension length for biological cross-links. As discussed in Section 2.4.3, there are existing frameworks for calculating corrections to the cross-linking free energy due to finite extensibility effects. Finite extensibility effects would become increasingly relevant at higher strains, so this might allow us to accurately predict a larger portion of the collagen stress-strain curve. Unfortunately modelling finite extensibility requires additional parameters that have not yet been well-determined experimentally, so an approach to estimating these parameters would need to be devised.

Throughout this work we have considered a constant constant density ρ within the fibril. This is likely a reasonable approximation for enzymatic cross-links, which are created during fibril formation. However for AGE-related cross-links, which are created long after fibril formation, we might expect the cross-linking density to be higher near the surface and lower in the core of the fibril [11]. To account for this, we would have to allow for a general density function $\rho(r)$. One possible approach could be to take $\rho(r,t) = \rho_{\text{enzymatic}} + \rho_{\text{AGE}}(r,t)$, where $\rho_{\text{AGE}}(r,t)$ is a solution to the 1D diffusion equation with the boundary conditions: $\rho_{\text{AGE}}(R,t) = \rho_{\text{AGE}}(-R,t) = 1$, and $\rho_{\text{AGE}}(r,0) = 0$ for $r \in (-R,R)$. It would then be possible to see how a fibril's elastic properties change with time as the density of AGE-related cross-links increases.

Bibliography

[1] Allen J Bailey. Structure, function and ageing of the collagens of the eye. *Eye*, 1(2):175, 1987.

[2] JS Bell, Sally Hayes, C Whitford, J Sanchez-Weatherby, O Shebanova, C Vergari, CP Winlove, N Terrill, T Sorensen, A Elsheikh, et al. The hierarchical response of human corneal collagen to load. *Acta biomaterialia*, 65:216–225, 2018.

[3] Arnab Bhattacharjee and Manju Bansal. Collagen structure: the madras triple helix and the current scenario. *IUBMB life*, 57(3):161–172, 2005.

[4] Laurent Bozec, Jaco de Groot, Marianne Odlyha, Brian Nicholls, Stephen Nesbitt, Adrienne Flanagan, and Michael Horton. Atomic force microscopy of collagen structure in bone and dentine revealed by osteoclastic resorption. *Ultramicroscopy*, 105(1-4):79–89, 2005.

[5] Laurent Bozec and Michael Horton. Topography and mechanical properties of single molecules of type i collagen using atomic force microscopy. *Biophysical journal*, 88(6):4223–4231, 2005.

[6] Aidan I Brown, Laurent Kreplak, and Andrew D Rutenberg. An equilibrium double-twist model for the radial structure of collagen fibrils. *Soft Matter*, 10(42):8500–8511, 2014.

[7] Mark R Buckley, Joseph J Sarver, Benjamin R Freedman, and Louis J Soslowsky. The dynamics of collagen uncrimping and lateral contraction in tendon and the effect of ionic concentration. *Journal of biomechanics*, 46(13):2242–2249, 2013.

[8] Markus J Buehler. Nature designs tough collagen: explaining the nanostructure of collagen fibrils. *Proceedings of the National Academy of Sciences*, 103(33):12285–12290, 2006.

[9] Samuel Cameron, Laurent Kreplak, and Andrew D Rutenberg. Polymorphism of stable collagen fibrils. *Soft matter*, 14(23):4772–4783, 2018.

[10] Samuel Cameron, Laurent Kreplak, and Andrew D Rutenberg. Phase-field collagen fibrils: Coupling chirality and density modulation. *Submitted to Physical Review Research*, 2019.

[11] Albert Daxer, Klaus Misof, Barbara Grabner, Armin Ettl, and Peter Fratzl. Collagen fibrils in the human corneal stroma: structure and aging. *Investigative ophthalmology & visual science*, 39(3):644–648, 1998.

[12] Baptiste Depalle, Zhao Qin, Sandra J Shefelbine, and Markus J Buehler. Influence of cross-link structure, density and mechanical properties in the mesoscale deformation mechanisms of collagen fibrils. *Journal of the mechanical behavior of biomedical materials*, 52:1–13, 2015.

[13] Pavel Dutov, Olga Antipova, Sameer Varma, Joseph PRO Orgel, and Jay D Schieber. Measurement of elastic modulus of collagen type i single fiber. *PloS one*, 11(1):e0145711, 2016.

[14] Russell Eberhart and James Kennedy. Particle swarm optimization. In *Proceedings of the IEEE international conference on neural networks*, volume 4, pages 1942–1948. Citeseer, 1995.

[15] KR Elder and Martin Grant. Modeling elastic and plastic deformations in nonequilibrium processing using phase field crystals. *Physical Review E*, 70(5):051605, 2004.

[16] Waltraud Folkhard, Daniela Christmann, Werner Geercken, Ernst Knörzer, Michel HJ Koch, Erika Mosler, Hedi Nemetschek-Gansler, and Theobald Nemetschek. Twisted fibrils are a structural principle in the assembly of interstitial collagens, chordae tendineae included. *Zeitschrift für Naturforschung C*, 42(11-12):1303–1306, 1987.

[17] John Galloway. Structure of collagen fibrils. In *Biology of Invertebrate and Lower Vertebrate Collagens*, pages 73–82. Springer, 1985.

[18] Alfonso Gautieri, Fabian S Passini, Unai Silván, Manuel Guizar-Sicairos, Giulia Carimati, Piero Volpi, Matteo Moretti, Herbert Schoenhuber, Alberto Redaelli, Martin Berli, et al. Advanced glycation end-products: mechanics of aged collagen from molecule to tissue. *Matrix Biology*, 59:95–108, 2017.

[19] SM Asif Iqbal, Dylan Deska-Gauthier, and Laurent Kreplak. Assessing collagen fibrils molecular damage after a single stretch–release cycle. *Soft matter*, 15(30):6237–6246, 2019.

[20] LD Landau, EM Lifshitz, JB Sykes, WH Reid, and Ellis H Dill. Theory of elasticity: Vol. 7 of course of theoretical physics. *Phys. Today*, 13:44, 1960.

[21] Y Mao. Finite chain-length effects in rubber elasticity. *Polymer*, 40(5):1167–1171, 1999.

[22] Y Mao, M Warner, EM Terentjev, and RC Ball. Finite extensibility effects in nematic elastomers. *The Journal of chemical physics*, 108(20):8743–8748, 1998.

[23] Chris J Peacock and Laurent Kreplak. Nanomechanical mapping of single collagen fibrils under tension. *Nanoscale*, 11(30):14417–14425, 2019.

[24] Andrew S Quigley, Stéphane Bancelin, Dylan Deska-Gauthier, François Légaré, Laurent Kreplak, and Samuel P Veres. In tendons, differing physiological requirements lead to functionally distinct nanostructures. *Scientific reports*, 8(1):4409, 2018.

[25] Andrew S Quigley, Stéphane Bancelin, Dylan Deska-Gauthier, François Légaré, Samuel P Veres, and Laurent Kreplak. Combining tensile testing and structural analysis at the single collagen fibril level. *Scientific data*, 5:180229, 2018.

[26] Werner Stille. Deformation of cholesteric elastomers by uniaxial stress along the helix axis. *The European Physical Journal E*, 28(1):57–71, 2009.

[27] M Warner and EM Terentjev. Nematic elastomersa new state of matter? *Progress in Polymer Science*, 21(5):853–891, 1996.

[28] M Warner, EM Terentjev, RB Meyer, and Y Mao. Untwisting of a cholesteric elastomer by a mechanical field. *Physical review letters*, 85(11):2320, 2000.

[29] Mark Warner and Eugene Michael Terentjev. *Liquid crystal elastomers*, volume 120. Oxford university press, 2007.

[30] Xiangjun Xing and Aparna Baskaran. Isotropic-cholesteric transition of a weakly chiral elastomer cylinder. *Physical Review E*, 78(2):021709, 2008.

[31] Noritaka Yamamoto. Tensile strength of single collagen fibrils isolated from tendons. *European Journal of Biophysics*, 5(1):1, 2017.

[32] Lanti Yang, Kees O Van der Werf, Carel FC Fitié, Martin L Bennink, Pieter J Dijkstra, and Jan Feijen. Mechanical properties of native and cross-linked type i collagen fibrils. *Biophysical journal*, 94(6):2204–2211, 2008.

Appendix A

A.1 Inverse of the Anisotropy Tensor

Lemma 1. Let $\boldsymbol{n} = [n_1, ..., n_k]$ be a k-dimensional vector such that $\sum_{i=1}^{k} n_i^2 = 1$. Then $\boldsymbol{n} \otimes \boldsymbol{n} = (\boldsymbol{n} \otimes \boldsymbol{n})^2$.

Proof. Note first that

$$\boldsymbol{n} \otimes \boldsymbol{n} = \begin{bmatrix} n_1^2 & n_1 n_2 & ... & n_1 n_k \\ n_1 n_2 & n_2^2 & ... & n_2 n_k \\ ... & ... & ... & ... \\ n_1 n_k & n_2 n_k & ... & n_k^2 \end{bmatrix}.$$

Thus,

$$\begin{aligned} (\boldsymbol{n} \otimes \boldsymbol{n})^2 &= \begin{bmatrix} n_1^2 & n_1 n_2 & ... & n_1 n_k \\ n_1 n_2 & n_2^2 & ... & n_2 n_k \\ ... & ... & ... & ... \\ n_1 n_k & n_2 n_k & ... & n_k^2 \end{bmatrix}^2 \\ &= \begin{bmatrix} n_1^2 \sum_{i=1}^{k} n_i^2 & n_1 n_2 \sum_{i=1}^{k} n_i^2 & ... & n_1 n_k \sum_{i=1}^{k} n_i^2 \\ n_1 n_2 \sum_{i=1}^{k} n_i^2 & n_2^2 \sum_{i=1}^{k} n_i^2 & ... & n_2 n_k \sum_{i=1}^{k} n_i^2 \\ ... & ... & ... & ... \\ n_1 n_k \sum_{i=1}^{k} n_i^2 & n_2 n_k \sum_{i=1}^{k} n_i^2 & ... & n_k^2 \sum_{i=1}^{k} n_i^2 \end{bmatrix} \\ &= \begin{bmatrix} n_1^2 & n_1 n_2 & ... & n_1 n_k \\ n_1 n_2 & n_2^2 & ... & n_2 n_k \\ ... & ... & ... & ... \\ n_1 n_k & n_2 n_k & ... & n_k^2 \end{bmatrix} = \boldsymbol{n} \otimes \boldsymbol{n}. \end{aligned}$$

□

Corollary 2. Let $\boldsymbol{n}$ be as in Lemma 1, and $\underline{\underline{\boldsymbol{\ell}}} = \ell_\perp(\underline{\underline{\boldsymbol{\delta}}} + [\zeta - 1]\boldsymbol{n} \otimes \boldsymbol{n})$. Then the inverse of $\underline{\underline{\boldsymbol{\ell}}}$ is given by $\underline{\underline{\boldsymbol{\ell}}}^{-1} = \ell_\perp^{-1}(\underline{\underline{\boldsymbol{\delta}}} + [\zeta^{-1} - 1]\boldsymbol{n} \otimes \boldsymbol{n})$.

Proof. Let $\underline{\underline{\boldsymbol{\ell}}}^{-1} = \ell_\perp^{-1}(\underline{\underline{\boldsymbol{\delta}}} + [\zeta^{-1} - 1]\boldsymbol{n} \otimes \boldsymbol{n})$, then

$$\begin{aligned}
\underline{\underline{\boldsymbol{\ell}}}\underline{\underline{\boldsymbol{\ell}}}^{-1} &= \ell_\parallel(\underline{\underline{\boldsymbol{\delta}}} + [\zeta - 1]\boldsymbol{n} \otimes \boldsymbol{n})\ell_\parallel^{-1}(\underline{\underline{\boldsymbol{\delta}}} + [\zeta^{-1} - 1]\boldsymbol{n} \otimes \boldsymbol{n}) \\
&= \underline{\underline{\boldsymbol{\delta}}} + [\zeta - 1]\boldsymbol{n} \otimes \boldsymbol{n} + [\zeta^{-1} - 1]\boldsymbol{n} \otimes \boldsymbol{n} \\
&\quad + [\zeta - 1][\zeta^{-1} - 1](\boldsymbol{n} \otimes \boldsymbol{n})^2 \\
&= \underline{\underline{\boldsymbol{\delta}}} + [\zeta + \zeta^{-1} - 2]\left(\boldsymbol{n} \otimes \boldsymbol{n} - [\boldsymbol{n} \otimes \boldsymbol{n}]^2\right).
\end{aligned}$$

As shown above, we have $\boldsymbol{n} \otimes \boldsymbol{n} = (\boldsymbol{n} \otimes \boldsymbol{n})^2$. Thus $\underline{\underline{\boldsymbol{\ell}}}\underline{\underline{\boldsymbol{\ell}}}^{-1} = \underline{\underline{\boldsymbol{\delta}}}$, which means $\underline{\underline{\boldsymbol{\ell}}}^{-1}$ is the inverse of $\underline{\underline{\boldsymbol{\ell}}}$. □

A.2 Stress-Strain Curve for an Isotropic Rubber

Consider an isotropic cross-linked elastomer (rubber), such that there is no dominant molecular director field ($\boldsymbol{n} = 0$), and no cross-linking anisotropy ($\zeta = 1$). From Equation 2.10, the free energy density for an isotropic cross-linked elastomer under strain is

$$f = \frac{1}{2}\mu \mathrm{Tr}\left[\underline{\underline{\boldsymbol{\lambda}}}^\top \cdot \underline{\underline{\boldsymbol{\lambda}}}\right]. \tag{A.1}$$

Note that for an isotropic rubber, there are no shear forces in a pure longitudinal extension, and so the strain field (in cylindrical (or cartesian) coordinates) is given by Equation 2.20. The free energy density is then

$$f = \frac{\mu}{2}\left(\frac{2}{\epsilon} + \epsilon^2\right). \tag{A.2}$$

Since this free energy density is independent of r, the free energy per unit volume is equal to the free energy density ($E = f$). Thus the longitudinal stress in the isotropic rubber due to the strain field is

$$\sigma = \frac{\partial E}{\partial \epsilon} = \frac{\partial f}{\partial \epsilon} = \mu\left(\epsilon - \frac{1}{\epsilon^2}\right). \tag{A.3}$$

A.3 Experimental Stress-Strain Curves

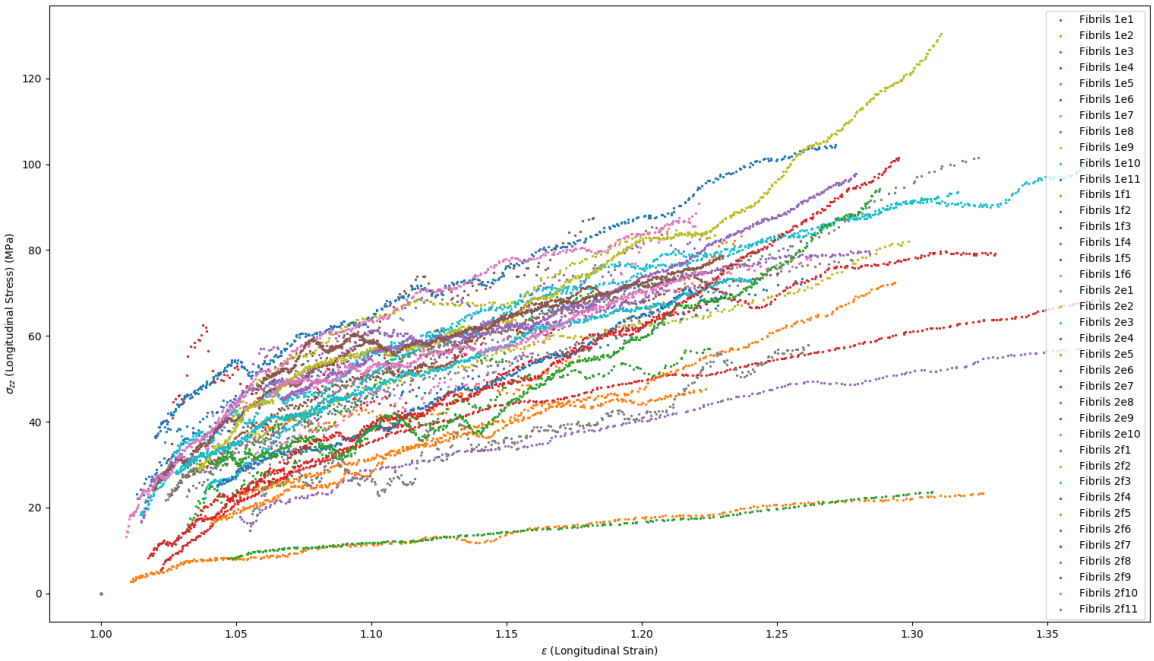

Figure A.1: Experimental Stress-Strain curves from [24]. We compare our model with 11 curves chosen to have radii matching what we take as the linear twist phase fibril radius.